Penetrator strength effect in long-rod critical ricochet angle [†]

K. Daneshjou[*] and M. Shahravi

Dep. of Mechanical Eng., Iran University of Science and Technology, Tehran, Iran

---

Abstract

3D numerical simulations were performed in order to further investigate the role of penetrator strength in the interaction of long-rods and oblique targets. Three distinctive regimes resulting from oblique impact depending on the obliquity, namely simple ricochet, critical ricochet and target perforation, were investigated in detail. Critical ricochet angles were calculated with a full 3D explicit finite element method for various impact velocities and strength of target plates and projectiles.

Numerical predictions were compared with existing two-dimensional analytical models and test results. It was predicted that critical ricochet angle increases with decreasing impact velocity and that higher ricochet angles were expected if higher strength target materials are employed. But there are differences between analytical models and 3D numerical simulation results or test results. The causes for these discrepancies are established by numerical simulations which explore the validity of the penetrator strength parameter in the analytical model as a physical entity.

As a matter of fact, in this paper we first investigate the role of penetrator dynamic strength using two-dimensional simulation which resulted in different penetrator strengths out of different impact velocities. Next, by applying these amounts for penetrator strength in Rosenberg analytical model the critical ricochet angle is calculated. Finally, a comparison between the present analytical method with the 3D simulation and test results shows that the new analytical approach leads to modified results with respect to Rosenberg ones.

Keywords: Critical ricochet angle; Penetrator strength; Numerical solution; Long-Rod

---

1. Introduction

It is well known that a projectile impacting on a suitably inclined surface can bounce back from the surface or partially penetrate it (without perforating it and being stopped by it) along a curved trajectory on the impacted surface with a reduced velocity [1]. This phenomenon, known as ricochet, is controlled by such factors as properties of the materials constituting the projectiles and the impacted surfaces, impact velocity of the projectiles, and relative obliquity of the surfaces with respect to the impact path of the projectiles, etc. [1]. Exploitation of ricochet to implement

mass efficient means of armour protection is common in many military applications [2]. Despite numerous researches on ricochet of various types of projectiles from various types of surfaces [3-13], critical conditions for the ricochet of long-rod type projectiles have not been completely established yet.

On the extension of the series of investigations on the impact of long-rods on targets [14-16], Tate first described ricochet using a simplified two-dimensional hydrodynamic model [6]. For the geometry shown in Fig. 1, it was predicted that ricochet of a projectile with a square cross section would occur if

$$\tan^3(\frac{\pi}{2} - \theta) > \frac{2}{3}\frac{\rho_p v^2}{Y_p}(\frac{L}{D} + \frac{D}{L})(1 + \sqrt{\frac{\rho_p}{\rho_t}}) \tag{1}$$

where θ is the oblique angle, ρ_p and ρ_t are densities of the projectile and the target, respectively,
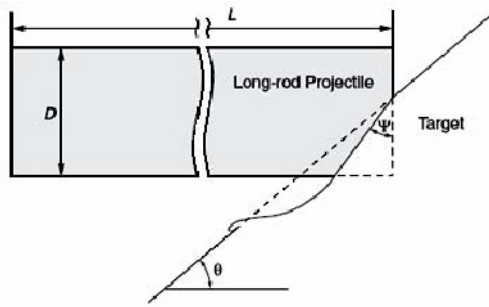
Fig. 1. Basic geometry used for simple two-dimensional analysis for ricochet of long-rod type projectiles by Tate [6] and Rosenberg et al [7].

v is the impact velocity, Yp is the dynamic strength of the projectile, and L and D are the length and diameter of the projectile, respectively. It is predicted from this expression that a higher projectile density, impact velocity and L / D ratio and lower rod strength will result in a lower ricochet angle.

However, in the derivation of Eq. (1), it was assumed that the projectile is a rigid body and that ricochet occurs due to the rotation of the projectile around its mass centre caused by the asymmetric reaction force exerted on its front from the impacted surface. These assumptions do not properly reflect physical phenomena predicted and observed in real systems, where the projectile bends on impact and then a plastic hinge forms, which travels backward with the progress of the projectile [1]. Further, Eq. (1) does not contain parameters representing geometry and mechanical properties of the target plate, which are believed to have some effects on the ricochet behaviour.

Rosenberg et al. [7] supplemented some of these shortcomings by further including the effect of target strength and bending of the projectile. The ricochet condition suggested by them is (see Fig. 1 for the geometry):

$$\tan^2(\frac{\pi}{2} - \theta) > \frac{\rho_p v^2}{R_t}(\frac{v+u}{v-u}) \qquad (2)$$

Where R_t is the dynamic yield strength of the target and u is the penetration velocity which is expressed as [6]:

$$u = \frac{\rho_p v - \sqrt{\rho_p^2 v^2 - (\rho_p - \rho_t)\{\rho_p v^2 + 2(Y_p - R_t)\}}}{\rho_p - \rho_t} \qquad (3)$$

Though the theoretical model developed by Rosenberg et al. includes the strength and density of both the target plate and the projectile, the L / D ratio of the projectile and thickness of the target plate are excluded. Comparison with experimental results showed that Eq. (2) formed a certain boundary between ricochet and penetration in terms of the ricochet angle expressed as a function of impact velocity, implying that the two-dimensional model could provide qualitative information regarding the ricochet condition.

However, recent numerical analysis by Zukas and Gaskill [9], in which differences in two-dimensional and three-dimensional calculations on the ricochet of a square projectile with L / D = 2 were compared, suggested that two-dimensional plane strain analysis with FEM codes overestimates the critical ricochet angles and therefore should not be used for design purposes.

Further development of the analytical model for a full three-dimensional geometry seems to be a formidable task due to the complexity of the physics involved in the ricochet, which includes large-scale high-strain-rate elastoplastic deformation of the projectile and the target plate together with the erosion of both occurring in a very short period of time [1]. Thus, alternative approaches, the use of experimental and numerical methods, have been used for more precise description of physical phenomena regarding ricochet by many researchers. Through a series of experiments on ricochet of long-rod projectiles made of modeling clay from a thick (undeformable) target, Johnson et al. [10, 11] observed the formation of an asymmetric elliptical crater on the target surface due to oblique impact of the projectile. Elongation and subsequent fragmentation of the projectile were also observed to occur after ricochet. Reid et al. [12] carried out experiments on the deformation behaviour of mild steel and aluminum long-rod projectiles striking at an undeformable oblique target and observed that the deformation of the projectiles consisted of impact end mushrooming and projectile buckling followed by its bending which terminated in a plastic hinge beyond which the projectile was not deformed. However, these experimental and numerical works were mainly concerned with ricochet phenomenology from the viewpoint of the projectile behaviour rather than critical ricochet condition such as ricochet angles.

We summarize a series of two-dimensional numerical simulations which were performed to study

the effects of material properties on the terminal ballistics of long-rod penetrators.

In this section an investigation on penetration velocity is done and variety of Y_p corresponding to different impact velocity is obtained. Successively the mentioned obtained amounts are taken to an analytical formula and the critical ricochet angle is calculated.

Some existing work on oblique impact [17-23] or near normal impact of the yawed projectiles [24-31] should also be noted. Although some useful information about the behaviour of the projectile and target during high-velocity impact can be obtained from these studies, they are focused more on the penetration and perforation process rather than the ricochet phenomena and, in particular, critical ricochet conditions. Especially, little attention has been paid to the problem of the modification of 2D critical ricochet angle analytical models. Thus, in the current study, ricochet phenomenology as well as the critical ricochet condition was numerically investigated for a real situation where a long-rod projectile impacts on oblique RHA and S-7 tool steel plates at various ordnance velocities. Experiments were also carried out to verify the numerical results from last papers.

2. Numerical analysis

2.1 Step1:

Existing ricochet models use a simplified two-dimensional hydrodynamic model [4] to predict penetration velocity; therfore, many simulations were performed in order to further investigate the role of penetrator strength in penetration velocity(u) at Eq.(4).

For the present purpose we used 2D simulations of tungsten alloy penetrators and RHA targets.

$$\frac{1}{2}\rho_p(v-u)^2 + Y_p = \frac{1}{2}\rho_t u^2 + R_t \qquad (4)$$

In order to avoid strain rate and strain hardening effect, a simple von-Mises yield criterion was used for both penetrator and target. Target yield strength (σ_{yt}) varied between 0.8 and 1.2 GPa(typical values for rolled homogeneous armor steels) and the penetrator's yield strength (σ_{yp}) varied in the 0.4- 1.6 GPa range. Five impact velocities were simulated: 1.2, 1.4, 1.6, 1.8 and 2 Km/s with L/D = 10.7 rods.

The output of each simulation was presented via the velocity histories of the eroding head of the penetrator(u) and its decelerating tail (v). These u(t) and v(t) data were used to plot the function A(t), which is defined by Tate[4] through his expression for the penetration velocity (u), using the modified Bernoulli equation:

$$u = \frac{v - \lambda(v^2 + A)^{1/2}}{1 - \lambda^2} \qquad (5)$$

Where $\lambda = \sqrt{(\frac{\rho_t}{\rho_p})}$ is the density ratio and A is defined by

$$A = \frac{2(R_T - Y_P)(1 - \lambda^2)}{\rho_t} \qquad (6)$$

These equations were used to extract an effective Y_P value for each case in the following manner: during the penetration process of long rod with finite strength, both its penetration velocity (u) and tail velocity(v) decrease with time. However, a measure for the steady-state nature of the process can be obtained by considering the time variation of A, as defined by Eq. (5). If A(t) turns out to be constant for most of the penetration process, one can use its value to define an effective strength for the penetrator (Y_P) through Eq. (6), since all the other parameters in this equation are known. The output from a typical simulation is given in Fig. 2 in terms of the time variations of u and v and the calculated function A(t) using Eq. (5). As is clearly seen, A(t) is relatively constant for times greater than about 20 μs in this simulation. This constant value of A is inserted in Eq. (6) to find Y_P , as described above and to calculate the ratio $\frac{Y_P}{\sigma_{yp}}$, where σ_{yp} is the value for the yield strength of the rod as used in the simulation. These variations of this ratio can help in finding the source(or sources) for the discrepancies between the one-dimensional model and the experimental data discussed above.

2.1.1 The dependence of Y_P on penetrator and target strengths

Fig. 3 presents the results for the variation of $\frac{Y_P}{\sigma_{yp}}$ vs. σ_{yp} for the two target strengths of 0.8 and 1.2 GPa. In both sets of simulations the impact velocity was kept at 1.8 Km/s and penetrator's strength varied
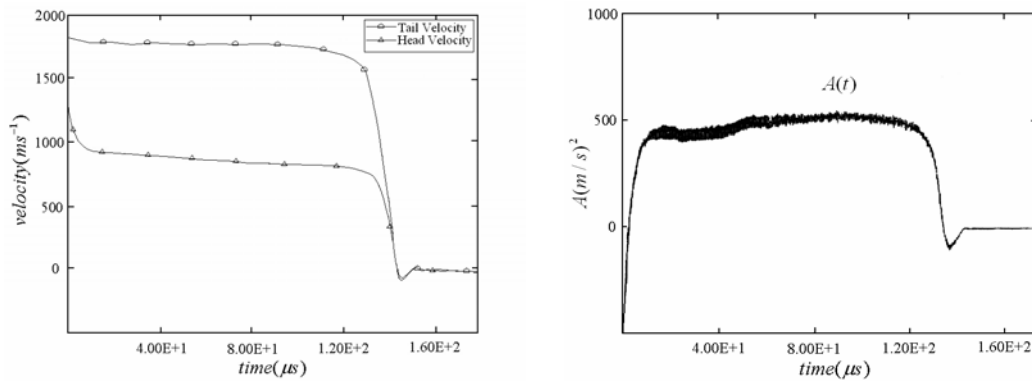
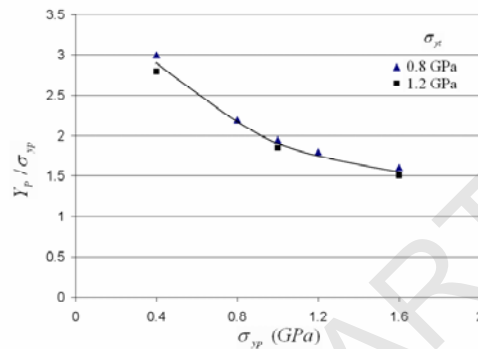Fig. 2. Typical results for the time variations of u, v and A.

Fig. 3. Simulation results for $\dfrac{Y_P}{\sigma_{yp}}$ vs. σ_{yp} for two target strengths (impact velocity is 1.8 Km/s).

in the 0.4-1.6 GPa range. All these simulations resulted in a relatively constant A(t) (for t>20 μs), as shown in Fig. 2, so that the computational error on Y_P is relatively small. Values of $\dfrac{Y_P}{\sigma_{yp}}$ in the range of 3-1.6 were obtained, as shown in Fig. 3, which is not surprising considering the fact that an empirical value of 2 is commonly used for this ratio in the 1D model. The closeness of the two sets of values for Y_P means that it is quite insensitive to target strength, which is what one expects from such a parameter.

The strong decrease of the ratio $\dfrac{Y_P}{\sigma_{yp}}$ with σ_{yp} is somewhat surprising considering the role of Y_P as a dynamic strength parameter, which is responsible for the deceleration of the penetrator. However, one can argue that this parameter contains other features in the interaction which are not manifested in the 1D model and the decrease shown in Fig. 3 includes the contributions of these features. One can conclude that,

with a proper functional dependence of Y_P on σ_{yp}, Y_P is a valid parameter in a one-dimensional model, at least as far as its sensitivity to both target and penetrator strengths is concerned.

2.1.2 The dependence of Y_P on impact velocity

In order to explore the velocity dependence of Y_P, another set of simulations was performed with L/D =10 rods (σ_{yp} =1.2 GPa) impacting the target (σ_{yt} =0.8 GPa) at velocities in the range of 1.2-2.0 Km/s. The Y_P values for these simulations are shown in Fig. 4 from which one clearly see the strong dependence of Y_P on impact velocity. This strong dependence is probably the main reason for the failure of the 1D model to reproduce the data. It is also worth noting that while for the higher velocities (1.8 and 2.0 Km/s) the A(t) curves exhibit a relatively flat plateau, it is less so for impact velocity of 1.4 Km/s. Moreover, the time dependence of A(t) is stronger for the higher strength penetrators and with σ_{yp} =1.6 GPa it was practically impossible to obtain even an

Table 1. critical ricochet angles.

Velocity (m/s)	1200	1400	1600	1800	2000
Y_P	1.6	1.8	2.0	2.2	2.36
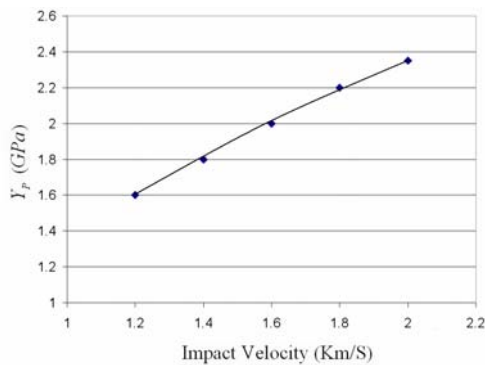
Fig. 4. The dependence of Y_P on impact velocity for σ_{yp} = 1.2 GPa and R_t = 0.8 Gpa.

average value of A(t). Thus, the primary penetration phase for these high-strength rods is far from a steady-state process in sharp contrast with the basic assumption behind the 1D model.

As Fig. 4 depicts in steady state penetration region, an increase of 200m/s in impact velocity causes a 0.2 in Y_P. Y_P values shown in table 1.

2.2 Step2:

In this case, a full three-dimensional explicit finite element analysis with Lagrangian formulation based on the principle of virtual work and the central difference time integration scheme [32,33] in Ls-dyna software was carried out to investigate the ricochet problem.

Fig. 5 shows a typical finite element model used in the numerical analysis. The model consists of a rectangular oblique target plate and a cylindrically shaped projectile with blunt nose shape that is initially located 1 mm away from the target. Only half of the whole geometry was modeled due to the inherent symmetry of the model along the x-direction of the coordinate as shown in Fig. 5. The length and diameter of the projectiles chosen for the numerical analysis were 75 and 7 mm, respectively, giving an L/D ratio of 10.7. Impact velocities of the projectiles were varied from 1000 to 2000 m/s with an increment of 250ms-l. Target plates modeled are l50mm long, 40mm wide and 6.25 mm thick. Obliquity of the plates was varied from 3° to 25° with intervals of 1°.
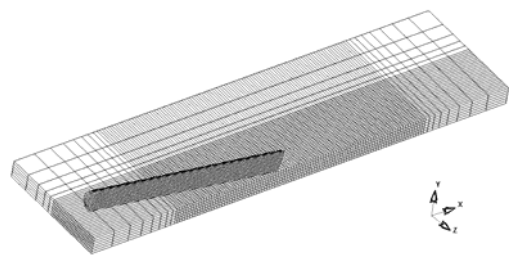

Fig. 5. Typical finite element mesh coordinate system used for the numerical study in this work.

Typical eight-node linear brick elements with reduced integration were used for meshing as shown in Fig. 5.

There are a number of factors that affect mesh integrity. These include element aspect ratio, element arrangement, uniform vs. graded meshes, and abrupt changes in meshes.

Ideally, calculations would be done with 1 : 1 aspect ratios in the elements. This hardly ever happens in practical 3-D calculations. Thus, it would be nice to know how the solution is affected when elements with aspect ratios exceeding 1 : 1 are used.

In order to test the mesh convergence in a numerical model, four set of different meshes were used. Calculations were performed with one (8338 elements), two (25880 elements), three (81720 elements) and four (187040 elements). calculations were done with an aspect ratio of 1 : 1 in impact zone of target. The critical ricochet angle as a function of impact velocity was compared with experimental results. With the exception of the lowest resolution, there was relatively little difference for the higher resolution calculations in terms of critical ricochet angle for the 3D calculations, but significant increases in CPU times were observed as resolution was enhanced. Therefore, the optimum model which leads to reliable results with maximum error of 8 percent and could save the run time is a model with 25880 elements. For this reason, the authors used this model in all simulations.

Material properties were applied to the model by assigning appropriate material properties to the predefined projectile and target element sets, i.e., properties of WHA to the projectile element set and properties of the two types of high hardness steel, namely, RHA class 4 [35] and S-7 tool steel [36], to the target element set.

In order to model a high-strain-rate mechanical response of the projectile and the target materials, a commonly used constitutive equation, the Johnson-

Cook equation [36], was used as it is known to describe high-velocity mechanical response of a number of metals fairly well [37]. This has the form

$$\sigma = \left(\sigma_0 + B\varepsilon_p^n\right)\left(1 + CLn\frac{\dot{\varepsilon}}{\dot{\varepsilon_0}}\right)\left[1 - \left(\frac{T - T_r}{T_m - T_r}\right)^m\right] \quad (7)$$

where σ_0 is the static yield strength, ε_p the effective plastic strain, ε the effective strain rate, ε_0 the reference strain rate, T the temperature, T_r the room temperature, T_m the melting temperature and B, C, m and n are material constants. For the materials used in this study, these parameters were determined from separate experiments (for RHA and WHA) or taken from Johnson and Cook (for S-7 tool steel) [36] and are shown in table 2 together with the basic physical properties required for the calculations.

The interaction between the projectile and the plate was simulated by a 3D Lagrangian-Lagrangian eroding contact algorithm based on a slave-grid/master segment concept.

Erosion of the projectile and the target was simulated through a so-called adaptive contact algorithm [38], which automatically updates contact definition between the interacting deformable bodies upon elimination of the elements when a pre-set level of plastic strains, determined by a separate depth of penetration (DOP) calibration, is reached. Pre-set level of plastic strain that was applied is 1.5. This value was obtained from many simulations from values 0.2 to 2 for strain.

For eroding contact, three parameters are defined as follows:

1- The boundary condition symmetry option parameter that determines whether a symmetry condition will be retained along a surface where elements fail.

2- The interior erosion option parameter that specifies whether erosion can subsequently occur along internal surfaces when the exterior surface fails.

3- The adjacent material parameter that determines

whether solid element faces are included for erosion along free boundaries.

Also Birth time value(contact surface becomes active at this time) set to 0 and Death time (contact surface is deactivated at this time) set to 1e20 μsec. Scale factor on default slave or master penalty stiffness set to 1.

Friction in Ls-Dyna is based on a Coulomb formulation. At this subject, an exponential interpolation function smooths the transition between the static, μ_s, and dynamic, μ_d, coefficients of friction where v is the relative velocity between the slave node and the master segment:

$$\mu = \mu_d + (\mu_s - \mu_d)e^{-c|v|} \quad (8)$$

Where

$$v = \frac{\Delta e}{\Delta t} \quad (9)$$

Δt is the time step size, c is a decay constant and typical values of friction, can be found in the Marks' Engineering Handbook. Coefficient of friction used in these simulations is equal to 0.32.

3. Experimental

Experiments were carried out to verify the numerical results. These results were used from earlier papers. The experimental set-up shown in Fig. 6 that was used in those papers consists of three witness blocks (38mm thick RHA class 4), an oblique target plate (6.25 mm thick RHA class 4), a velocity-measuring device and a solid propellant gun. WHA projectiles with L / D ratios of 10.7 *(L* = 75 and D = 7 mm) were impacted at velocities of about 1000 and 1500 ms^{-1}. The velocities of the projectiles were controlled by adjusting the amount of solid propellant charge. The relations between the amount of the charge and the projectile velocities were calibrated in a preparatory experiment.[43]

Table 2. Material properties and constants for the Johnson-Cook model applied to the numerical model.

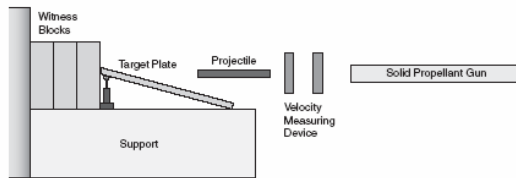|	Shear modulus (GPa)	$\rho(kgm^{-3})$	Specific heat ($Jkg^{-1}K^{-1}$)	$T_m(K)$	$\sigma_0(MPa)$	$B(MPa)$	n	C	m
WHA	152.02	17000	134	1723	1410	223.3	0.11	0.022	1.0
RHA	76.96	7840	477	1809	1160	415.9	0.28	0.012	1.0
S-7	79.96	7750	477	1763	1539	477	0.18	0.012	1.0

Fig. 6. Schematic illustration of the experimental set-up for the observations of oblique impact of a long-rod projectile on a steel target plate performed in this study.[43]

4. Results and discussion

4.1 Post-impact behaviour of the projectile and the target plate

Numerical results are graphically shown in Figs. 7-9 in terms of the mesh deformation with the lapse of time to analyse the behaviour of the WHA projectile and the RHA target with thickness comparable to the projectile diameter during the oblique impact. When the projectile impact velocity is 1000 ms^{-1} and the target oblique angle is 10°, as in the case shown in Figs. 7-9, the projectile initially bends on impact (Fig. 7a). Subsequently, a plastic hinge is formed which remains at the initial point of impact with respect to a fixed coordinate system (Eulerian) resulting in its relative backward motion along the x-direction of the coordinate system (Fig. 5) as the projectile progresses forward [Figs. 7(b)-7(d)]. In the case being considered (θ = 10°), where the oblique angle is lower than the critical ricochet angle, the target does not deform much and no significant erosion of the impacted surface is noticed whilst the front end (denoted as head hereinafter) of the projectile lifts from the target surface after sliding some distance and eventually the projectile bounces away [Figs. 7(e)-7(h)]. Such behaviour is yielded due to the asymmetric reaction force exerted from the contact area to the projectile, which is reportedly proportional to the area of the contact, target strength and oblique angle [6, 7, 12].

When the oblique angle of the target plate is increased to 12° while keeping the impact velocity the same, the projectile shows somewhat different behaviour. As shown in Figs. 8(a)-8(d), it initially pushes the impacted area of the target inward following impact since the target plate is allowed.

While the head of the projectile tends to bounce back from the target due to the reaction force exerted from the contact area at the initial stage of the impact, its trailing portion (denoted as tail hereinafter) tends

to penetrate into the target along an almost identical trajectory of the initial impact [Fig. 8(e)]. Consequently, the front part ahead of the plastic hinge, which was bent and slid on the plate surface, bounces away while the rear part behind it penetrates into the deformed target forming a stretched section in the projectile and an impact crater in the target [Figs. 8(f) and 8(g)]. Indeed, the relatively thin deformable target plays a significant role in yielding such phenomena. At the critical oblique angle, the tail also bounces away at a later time step before it completely perforates the target achieving critical ricochet [Fig. 8(h)]. At this stage the elongation of the projectile becomes so severe that it results in the fragmentation of the projectile.

When the oblique angle is further increased to 14° beyond the critical angle, as can be seen in Figs. 9(a)-9(d), the initial behaviour of the projectile and the target is similar to the case of critical ricochet shown in Figs. 8(a)-8(d).

However, unlike in the previous case, the tail part further progresses to penetrate into the target downward by eroding it [Figs. 9(e) and 9(f)], resulting in the fragmentation of the projectile due to extreme elongation as well as complete penetration (perforation) of the target as shown in Figs. 9(g) and 9(h).

Understanding the physical nature of the above behaviour of the projectile and the target can be supplemented by analysing the changes in the projectile velocities after impact, as has also been performed for normal penetration in the literature [39-41]. For this purpose, post-impact changes in the horizontal (along the x-direction) and vertical (along the y-direction) velocities of head and tail of the projectile have been monitored during the numerical calculations and the results are plotted in Figs. 10-15. Before impact, the head and the tail move at the same initial velocity of 1000 ms $^{-1}$ and there is no vertical velocity term. For a relatively low oblique angle, e.g., θ = 10°, as shown in Figs. 10 and 11, the horizontal velocities of the head and the tail of the projectile after impact are kept almost identical, implying no significant axial strain, which prevents projectile segmentation. It can also be seen that the horizontal velocities did not decrease noticeably. From this, it is inferred that the projectile does not encounter any significant resistance to its motion along the flight trajectory, and that the impact interaction of the projectile with the target does not cause any large-scale deformation of the target.
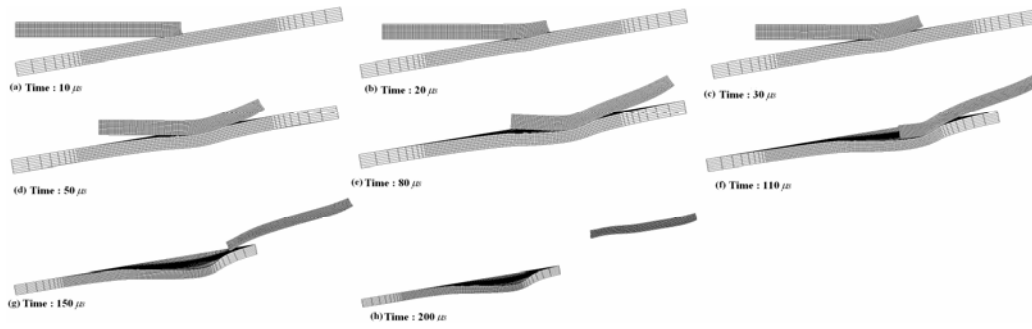
Fig. 7. Numerical results showing the behavior of the WHA projectile and the RHA target when the oblique angle is 10° an.d the impact velocity is 1000 m/s.
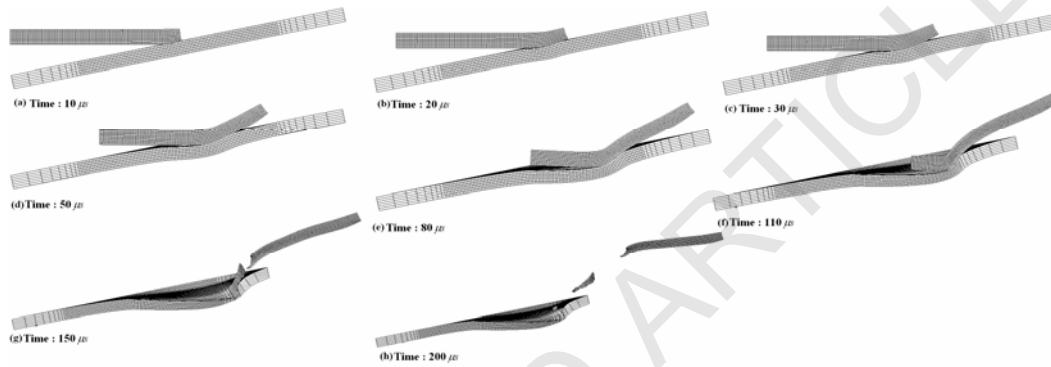

Fig. 8. Numerical results showing the behavior of the WHA projectile and the RHA target when the oblique angle is 12° and the impact velocity is 1000 m/s.
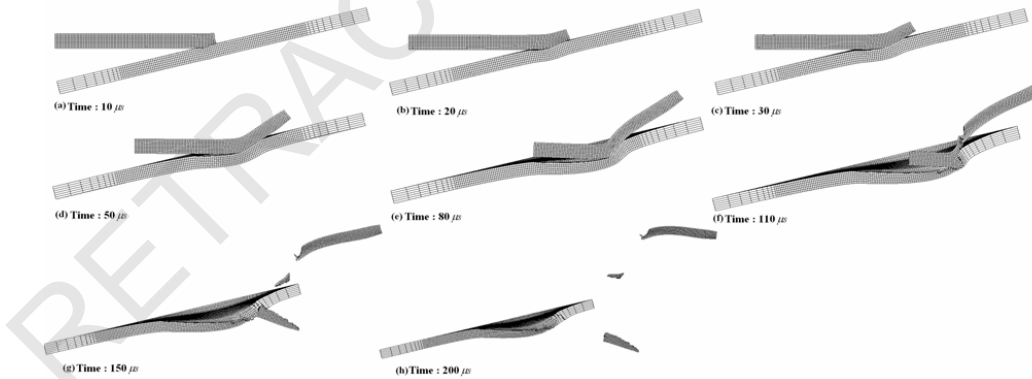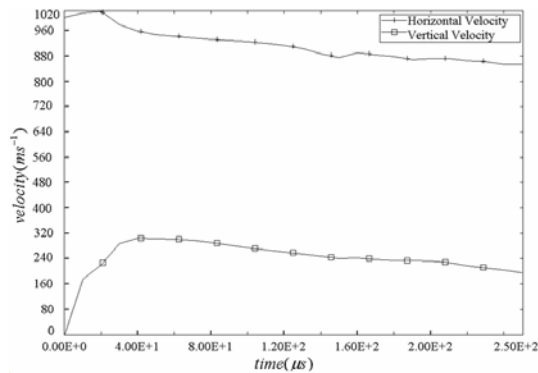

Fig. 9. Numerical results showing the behavior of the WHA projectile and the RHA target when the oblique angle is 14° and the impact velocity is 1000 m/s.

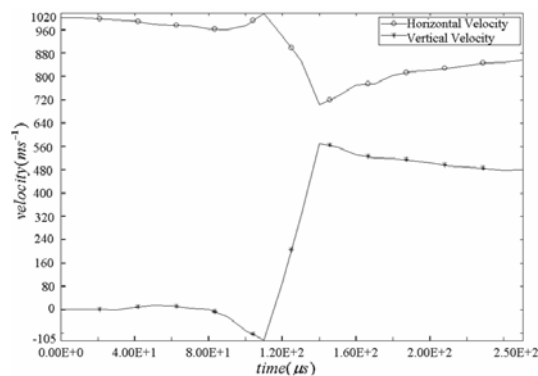Fig. 10. Projectile head horizontal and vertical velocity ($\theta = 10°$).

Fig. 11. Projectile tail horizontal and vertical velocity ($\theta = 10°$).

While there were only slight changes in the horizontal velocities, the vertical velocities of the head and the tail undergo noticeable changes during the impact process. As can be seen in Fig. 10, the vertical velocity of the head initially increases to about 300 ms^{-1} and remains almost the same thereafter, which would be associated with sliding on the target surface and subsequent takeoff of the head shown in Fig. 7. On the other hand, the vertical velocity of the tail is almost 0 until about 80 μs and then increases to about 550 ms^{-1} at 140 μs. This indicates that the impact of the head on the target does not cause any yawing force in the rear part of the projectile which is beyond the plastic hinge mentioned above. Near-constant vertical tail velocity of 460 ms-l after about 160 μs would indicate the takeoff of the tail as shown in Figs. 7(f) and 7(h).

However, where critical ricochet was achieved ($\theta = $ 12° for the case considered herein), as shown in Fig. 12, the decrease in the horizontal velocity of the

head with respect to time is more pronounced than in the previous case, indicating that the progress of the head is hindered more. In particular, as shown in Fig. 13, the horizontal velocity of the tail decreases to almost 0 from about 140 μs, producing a velocity difference between the head and the tail of about 750 ms^{-1}. Such a large velocity difference may cause large-scale deformation and therefore it would explain the stretching of the projectile shown in Fig. 8(g) followed by the segmentation of the projectile shown in Fig. 8(h). At the same time, a sudden drop in the horizontal velocity of the tail between 100 and 150 μs is believed to be related to the target cratering shown in Figs. 8(f) and 8(g), which could exert a high resistance to the advance of the tail. When critical ricochet is achieved, even though the impact crater is formed on the target, this does not lead to target perforation. This can be explained from the changes in the vertical velocities of the head and the tail shown in Figs. 12 and 13, where it can be seen that the head and the tail sequentially acquire positive, vertical velocity components. They begin to take off from the target plate at about 0 and 150 μs, respectively, indicating no further penetration of the target.

A similar trend is obtained when the target oblique angle is further increased, e.g., θ = 14°, as shown in Figs. 14-15 while two apparent differences are noticed. First, the horizontal velocity of the head, once it is decreased to about 700 ms^{-1} at about 120 μs, remains nearly constant implying that the flight of the head portion is no longer hindered by the target thereafter, probably due to the earlier segmentation of the projectile. In the previous case shown in Fig. 12, the head portion was connected to the tail portion through the elongated portion until the later time step so that the tail, still staying in the impact crater in the target, delayed the propagation of the head, which is represented as continuously decreasing velocity. Second, the behaviour of the tail after segmentation is completely different: the vertical velocity of the tail decreases to a negative value of about -180 ms^{-1} from about 150 ms^{-1}, which is then maintained almost constant after about 180 μs. This indicates that the fragmented tail is heading downward, which would be responsible for the perforation of the target shown in Fig. 9(h).

The post-impact behaviour of the deformable projectile and the deformable target with finite thickness described so far in general agrees qualitatively with what has been observed and predicted in the previous
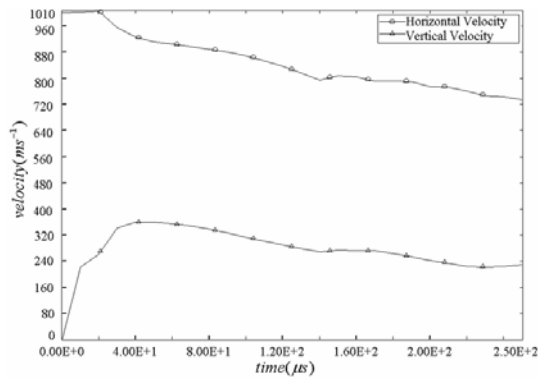
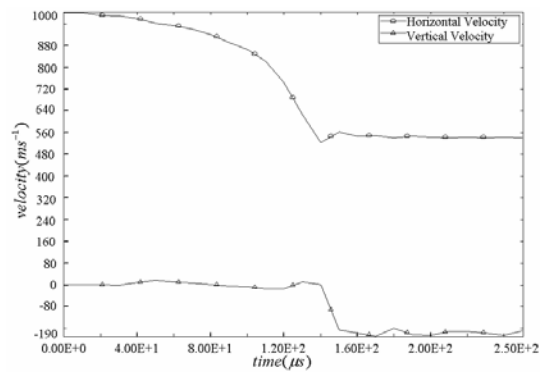Fig. 12. Projectile head horizontal and vertical velocity ($\theta = 12°$).
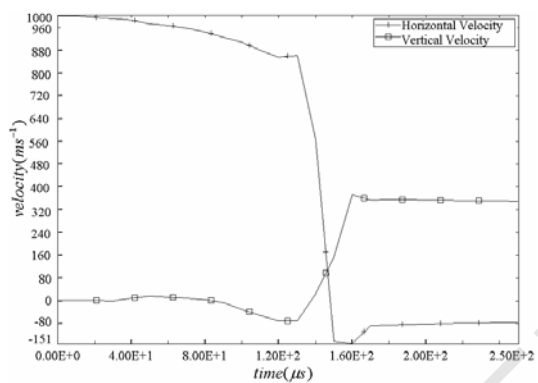

Fig. 13. Projectile tail horizontal and vertical velocity ($\theta = 12°$).

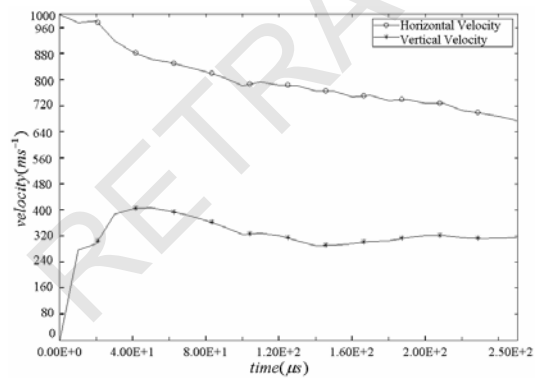Fig. 14. Projectile head horizontal and vertical velocity ($\theta = 14°$).

Fig. 15. Projectile tail horizontal and vertical velocity ($\theta = 14°$).

works in which ricochet occurred at undeformable (and sometimes rigid) target surfaces [6-12]. However, as apparent in Figs. 7-9, the inward deformation of the target plate due to the finite thickness comparable to the projectile diameter is shown to assist the segmentation of the projectile, followed by the perforation of the target plate by the broken rear part of the projectile. Such phenomena could be responsible for the difficulty of obtaining ricochet from relatively thin plates.

Senf *et al.* [8] showed how the ricocheting rod can form a plastic hinge at the impact site to deflect the rod from a rigid target surface. These test results (see Fig. 20) are similar to FEM solution results as shown in Figs. 7 to 9. But in FEM solution the target plate is not rigid and it deflected more.

4.2 Critical ricochet angles

In accordance with the definition of ricochet mentioned in the introduction, changes in the critical ricochet angles were derived by analysing the numerical results graphically in the manner described in last section and were plotted as functions of impact velocities in Fig. 16 for the RHA target plate. The ricochet angle curves shown in Fig. 16 were obtained from curve-fitting the numerical results as a first-order exponential decay function. The fitted equations, their parameter values, and the statistical analysis of the fitted results are also reported in the figure. The numerical results are confirmed with experimental results as shown in Fig. 16. In Fig. 16, the hollow circle markers indicate perforation of the RHA target plate by the long-rod projectile while the solid star markers indicate critical ricochet of the projectile. It can be seen that there is good agreement between the two.
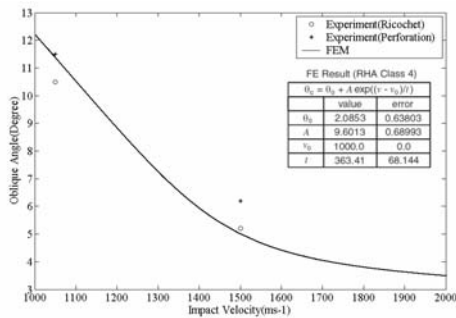
Fig. 16. Comparison of the numerically predicted critical ricochet angles for various velocities with the experimental results.

Fig. 17. Comparison of the numerically determined critical ricochet angles for various velocities with those predicted from two dimensional analytic models of Tate[6] and Rosenberg et al. [7].
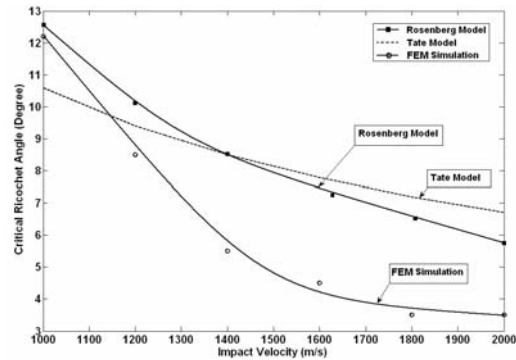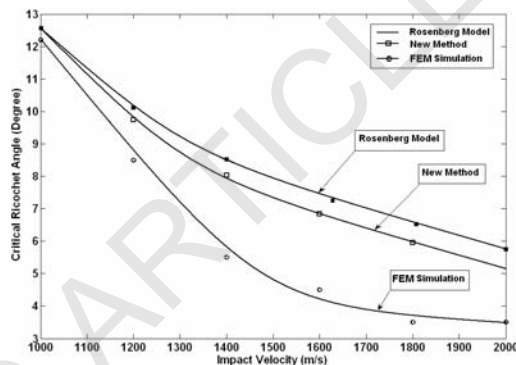

Fig. 18. Comparison of the numerically determined critical ricochet angles for various velocities with those predicted from two dimensional analytic models of Rosenberg et al. [7] and new method.

It is noticed in Fig. 16 that the critical ricochet angle falls with increasing impact velocities. In other words, at a low target oblique angle, the ricochet can be achieved up to relatively high impact velocities though the penetration capability in flight direction is high at such velocities, i.e., ricochet is easily achieved with a low oblique angle. On the other hand, when the target oblique angle is high, the ricochet is possible only up to a limited impact velocity beyond which full penetration (perforation) occurs.

Such a trend of increasing ricochet angles with lower impact velocities can be understood from the pressure (or axial stress) developed at the projectile-target interface, known as Tate pressure, which takes the form of a modified Bernoulli equation as [14, 15, 41]:

$$P = \frac{1}{2}\rho_p(v-u)^2 + Y_p = \frac{1}{2}\rho_t u^2 + R_t \qquad (10)$$

The numerical results on the critical ricochet angles are also compared with existing two-dimensional analytical models developed by Tate [6] and Rosenberg et al. [7], independently. The critical ricochet angles based on these models have been calculated for a WHA long-rod projectile and an RHA target as functions of impact velocities in Fig. 17. Also shown are the corresponding numerical results. It can be seen in the figure that the Tate model overestimates the critical ricochet angle for impact velocities higher than 1170 ms^{-1} and *vice versa* for lower velocities. Further, the slope of the Tate curve is different from the numerical one: the difference in the two curves becomes larger as the velocity of interest either increases or decreases from 1170 ms^{-1}. On the other hand, the model developed by Rosenberg et

al. shows a similar trend to the numerical results, though the former overestimates the critical ricochet angles at all impact velocities. As is shown in Fig. 17, by use of the current framework, presented in this paper, the discrepancies between the Rosenberg method, simulation and test result can be diminished up to 20 percent.

4.3 Effects of the target strength

While the RHA has been widely used as a primary armour material over decades, in some cases, stronger material such as high hardness armour (HHA) has also been adopted, though its use is limited due to lower toughness. To investigate the effect of material strength on the ricochet angle, material constant terms in the Johnson-Cook model for S-7 tool steel, which has static yield strength and hardness similar to HHA

produced by ThyssenKrupp AG, were taken from the literature [36] and applied to the numerical model. The ricochet angles calculated for S-7 tool steel were plotted as a function of the impact velocity in Fig. 19. It can be seen that a higher ricochet angle is predicted for a given impact velocity if the target strength is increased. Such behaviour is explained by examining the one-dimensional hydrodynamic penetration model described in Eq. (10). It was reported that the dynamic yield strengths of S-7 tool steel and RHA are about 6.2 and 5.3 GPa, respectively [42]. Thus, at a given impact velocity, the use of the high hardness plate, S-7 tool steel, would foster the ricochet of the projectile, i.e., the target plate can tolerate more vertical component of the projectile movement. This implies that a target plate with higher strength allows a higher oblique angle for the ricochet of the projectile at a given velocity.

It is further noticed in Fig. 19 that there is a salient increase in the ricochet angle especially at low impact velocities as the material strength increases whilst improvement in ricochet capability through the use of stronger materials gradually decreases at higher velocities. Such a trend is qualitatively predicted when the constant in Eq. (7), which is related to the dynamic strength of the target material, is changed to a higher one for the S-7 tool steel.

5. Summary and conclusions

Ricochet of a WHA long-rod projectile impacting on oblique, steel target plates with finite thickness was investigated numerically by using a full, three-dimensional, explicit finite element method. Effects of the impact velocities of the projectiles and the hardness of the projectiles and targets on the critical ricochet angle were considered.

Numerical study results were supported by experimental observations of last papers. The post-impact behaviour of the deformable projectile and deformable target with finite thickness in this work in general agreed qualitatively with previous work based on undeformable (and rigid) target surfaces. However, the deformable target assisted the breakage of the
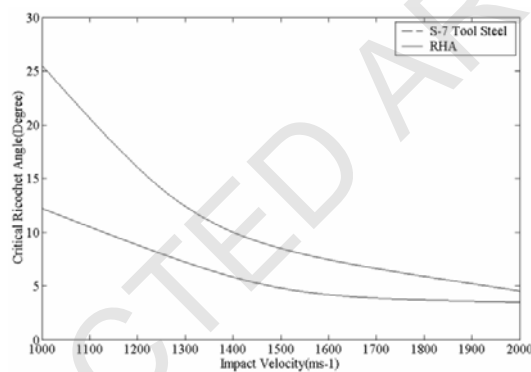

Fig. 19. Effect of target strength on the critical ricochet angles.
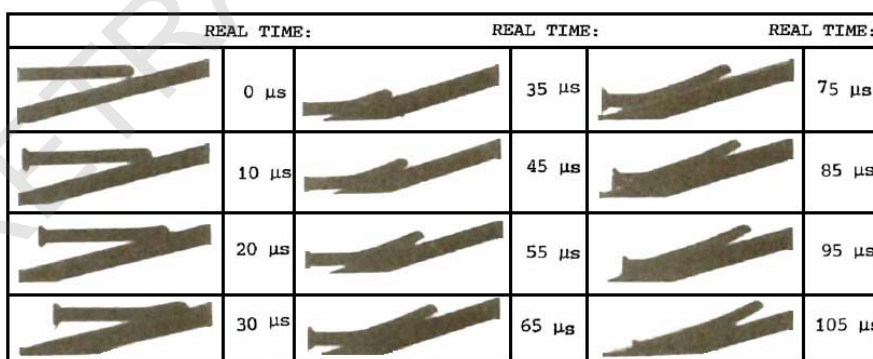

Fig. 20. Spark cinematography of a ricocheting rod projectile[34].

projectile followed by the perforation of the plate by the broken rear part of the projectile.

For the cases considered herein, the numerical study predicted that the critical oblique angle of the target plates required for ricochet of long-rod type projectiles rises with lower projectile velocity and the prediction was shown to be reliable by experimental results. This trend itself is consistent with a two-dimensional analytical model, while it was suggested that the two-dimensional results are an overestimation, which is qualitatively consistent with the results of Zukas and Gaskill [9].

According to two-dimensional simulations of penetration phenomenon, it is observed that the penetrator dynamic strength depends on impact velocity magnitude. These newly obtained amounts are taken into account, which leads to a closer coincidence between calculated critical ricochet angle and the test results. One other significant advantage of this method is lowering the error between test results and the Rosenberg analytical method in calculation of critical ricochet angle.

When the target hardness was considered, the numerical results predicted that a higher ricochet angle could be obtained by employing harder target materials for a given impact velocity, which was appreciable at lower velocities in particular.

Refrences

[1] J. A. Zukas, High Velocity Impact Dynamics, Wiley, (New York), (1990).

[2] R. M. Ogorkiewicz, Technology of Tanks, Coulsdon: Janes's Information Group, (1991).

[3] W. Goldsmith and P. M. Cunningham, Kinematic Phenomena Observed During the Oblique Impact of a Sphere on a Beam, *J. Appl. Mech.*, (Trans. ASME), (1956) 78 612.

[4] R. F. Recht and T. W. Ipson, The dynamics of terminal ballistics, Final Report No AD274128 (Denver: Denver Research Institute), (1962).

[5] S. A. Finnegan, L. F. Dimaranan, D. E. R. Heimdahl and J. K. Pringle, A study of obliquity effects on perforation and ricochet processes in thin plates impacted by compact fragments, Proc. 14th Int. Symp. Ballistics, (1993) p 661.

[6] A. Tate, A simple estimate of the minimum target obliquity required for the ricochet of a high speed long rod projectile, *J. Phys. D: Appl. Phys.*, (1979) 12 1825.

[7] Z. Rosenberg, Y. Yeshurun and M. Mayseless, On the. Ricochet of long rod projectiles, Proc. 11th Int. Symp. Ballistics, (1989) p. 501.

[8] H. Senf, H. Rothenhausler, F. Scharpf, A. Both and W. Pfang, Experimental and numerical investigation of the ricocheting of projectiles from metallic surfaces, Proc. 6th Int. Symp. Ballistics, (1981) p. 510.

[9] J. A. Zukas and B. Gaskill, Ricochet of deforming projectiles from deforming plates, *Int. J. Impact Eng.* (1996) 18 601.

[10] W. Johnson, A. K. Sengupta and Ghosh, High velocity oblique impact and ricochet mainly of long rod projectile: an overview, *Int. J. Mech. Sci.*, (1981) 24 425.

[11] W. Johnson, A. K. Sengupta and Ghosh, Plasticine modeled high velocity oblique impact and ricochet of long-rods, *Int. J. Mech. Sci.*, (1981) 24 437-455.

[12] S. R. Reid, A. J. Edmonds and W. Johnson, Bending of long steel and aluminum rods during end impact with a rigid target, *J. Mech. Eng. Sci.*, (1981) 23 85.

[13] G. H. Jonas and J. A. Zukas, Mechanics of penetration: analysis and experiment, *Int. J. Eng. Sei.* , (1978) 16 879.

[14] A. Tate, A theory for the deceleration of long rods after impact, *J. Mech. Phys. Solids.*, (1967) 15 387.

[15] A. Tate, Further results in the theory of long rod penetration, *J. Mech. Phys. Solids*, (1969) 17 141-150.

[16] A. Tate, A simple estimate of the minimum target obliquity required for the ricochet of a high speed long rod projectile. *Int. J. Mech. Sci.*, (1977), 19, 661-671.

[17] W. Goldsmith and S. A. Finnegan, Normal and oblique impact of cylindro-conical and cylindrical projectiles on metallic plates, *Int. J. Impact Eng.*, (1986) 4 83.

[18] E. Roecker and C. Grabarek, The Effect of Yaw and Pitch on Long Rod Penetration into Rolled Homogeneous Armor at Various Obliquities, Proc. 9th Int. Symp. Ballistics, (1986) 2 467-473.

[19] J. Falcovitz, M. Mayseless, Z. Tauber, D. Keck, R. Kennedy, K. Ofstedhal and P. Sing, A Computer Model for Oblique Impact of a Rigid Projectile at Ductile Layered Targets, Proc. 11th Int. Symp. Ballistics, (1989) p. 311.

[20] G. R. Johnson, R. A. Stryk, T. J. Holmquist and O. A. Souka, Recent EPIC code developments for high velocity impact: 3D element arrangements and 2D

fragment distributions, *Int J Impact Eng* , (1990), 281–294.

[21] I. G. Cullis and N. J. Lynch, Performance of model scale long rod projectiles against complex targets over the velocity range 1700-2200 m/s, *Int. J. Impact Eng.*, (1995) 17 263-274.

[22] G. Luttwak, Z. Rosenberg and Y. Kivity, Long rod penetration in oblique impact, AlP Conf Proc.(1996).

[23] E. Pierazzo and H. J. Melosh, Understanding oblique impacts from experiments, observations, and modeling, *Ann. Rev. Earth Planet. Sei.*, (2000) 28 141-167.

[24] V. Hohler and A. J. Stilp, Interferometric Investigation of Rod Deceleration During Impact Process, Proc. 6th Int. Symp. Ballistics, (1981) p. 333.

[25] G. F. Sislby, Penetration of semi-infinite steel targets by tungsten rods at 1.3 to 4.5 lcds, Proc. 8th Int. Symp. Ballistics, (1984) p. 31.

[26] D. J. Cagliostro, D. A. Mandell, L. A. Schwalbe, T. F. Adams and E. J. Chapyak, Armor penetration by projectile with combined obliquity and yaw, *Int. J. Impact Eng.*, (1990) 10 81-92.

[27] T. W. Bjerke, G. F. Silsby, D. R. Scheffler and R. M. Mudd, Yawed long-rod armor penetration, *Int. J. Impact Eng.*, (1992) 12 281-292.

[28] Y. I. Bukharev and V. I. Zhukov, Model of the penetration of a metal barrier by a rod projectile with an angle of attack, Combustion, Explosion and Shock Waves, Comb. Expl. Shock Waves (Fiz. Goren. Vzryva), (1995) 31 362.

[29] W. Goldsmith, E. Tam and D. Tomer, Yawing impact on thin plates by blunt projectiles, *Int. J. Impact Eng.*, (1995) 16 479-498.

[30] C. E. Anderson, S. J. Bless, T. R. Sharron, S. Satapathy and M. J. Normandia, Investigation of yawed impact into a finite target, AlP Conf Proc., (1998) p. 925.

[31] M. Lee and S. J. Bless, Cavity models for solid and hollow projectiles, AlP Conf Proc., (1998) 925-928.

[32] C. Zienkiewicz and R. L. Taylor, *The Finite Element Method* 4th edn, McGraw-Hill, (New York), (1991) vol 2.

[33] T. Belytschko, W. K. Liu and B. Morgan, *Nonlinear Finite Elements for Continua and Structures,* Wiley, (New York), (2000).

[34] W. Goldsmith, Non-ideal projectile impact on targets, *Int. J. Impact Eng,* (1999). 22 95 395.

[35] US DoD *Armour Plate, Steel, Wrought, Homogeneous* Military Specification MIL-A-12560H (Amendment 3), (2000).

[36] G. R. Johnson and W. H. Cook, A constitutive model and data for metals subjected to large strains, high strain rates and high temperatures. Proceedings of the 7th International Symposium on Ballistics, (1983) p. 541.

[35] M. A. Meyers, *Dynamic Behavior of Materials* Wiley, (New York), (1994).

[36] LsDyna User's Manual version 970, (Livermore Software Technology Corporation), (2007).

[37] Z. Rosenberg and E. Dekel, A computational study of the relations between material properties of long-rod penetrators and their ballistic performance, *Int. J. Impact Eng,* (1998), 21 283 296.

[38] C. E. Anderson, J. D. Walker, S. J. Bless and Y. Partom, On the L/D effect for long-rod penetrators, *Int. J. Impact Eng,* (1996). 18 247 264.

[39] C. E. Anderson and J. D. Walker, An examination of long-rod penetration, *Int. J. Impact Eng,* (1991) 11 481 501.

[40] C. E. Anderson, J. D. Walker and G. E. Hauver, Target resistance for long-rod penetration into semi-infinite targets, *Nucl. Eng*, (1992) 138 p. 93-104.

[41] L. Woong , J. L. Heon and S. Hyunho, Ricochet of a tungsten heavy alloy long-rod projectile from deformable steel plates, *Int. J. Appl,Phys*, (2002) 35.

Kamran Daneshjou, is University Professor at Iran University of Science and Technology. He studied his MSC and PhD at aeronautical Engineering de-partment of Imperial college of Science and Technology in London.

His own research is at the interface of solid mechanic, finite element and electromagnetic lunchers to address the sustainable development of aerospace and solid mechanic projects. His publications include 7 books and over 100 scientific papers.